Adsorption (2024) 30:1175–1191
https://doi.org/10.1007/s10450-024-00487-2

Computational exploration of SF_6 adsorption and decomposition on SiGe and calcium-decorated SiGe surfaces

Jabir H. Al-Fahemi[1] · **Kamal A. Soliman**[2]

Received: 8 December 2023 / Revised: 5 May 2024 / Accepted: 6 May 2024 / Published online: 25 May 2024

Abstract
This study investigates the sensitivity and selectivity of gas adsorption (SF_6, SO_2F_2, SOF_2, SO_2, and HF) on SiGe surfaces and Ca atom-decorated SiGe surfaces using Density Functional Theory (DFT). The optimized structures, bond lengths, and angles of the gas molecules are analyzed, providing valuable insights into their geometric features and bonding configurations. For every gas on both surfaces, important variables such as adsorption energy, and charge transfer are examined. In particular, there is a significant increase in charge transfer and adsorption energy when SF_6 interacts with Ca$2D-SiGe as opposed to the SiGe surface. To emphasize changes in band gap and electronic structure, the study explores electronic properties such as density of states (DOS) and projected density of states (PDOS) spectra before and after gas adsorption. Electron density differences (EDD) analysis is used to clarify the type of interactions, including accumulation and depletion of charge. The results reveal that all gases except HF/ Ca$2D-SiGe showed chemical adsorption. The study also takes into account recovery time, an important metric for sensor materials, which is calculated for the breakdown gases of SF_6 on both surfaces at different temperatures and shows potential uses for gas detection. Future research should focus on a broader range of gas molecules and their interactions with SiGe and Ca-decorated SiGe surfaces. Ultimately, the integration of SiGe-based sensor devices in real-world applications such as environmental monitoring, industrial safety, and medical diagnostics can be explored to understand the broader potential of these materials in the field of gas detection.

Keywords Density functional theory · SiGe Surface · Ca Atom-Decorated SiGe Surfaces · SF_6 decomposition gases · Adsorption · Electronic properties

1 Introduction

Sulfur hexafluoride (SF_6) is a non-toxic gas that is commonly utilized in industrial, medical diagnostics, and electrical applications. SF_6 is utilized as an insulating gas in high-voltage electrical equipment such as switchgear, transformers, and circuit breakers due to its excellent thermal conductivity, arc-extinguishing properties, and high dielectric strength [1–9]. SF_6 serves a dual purpose in industrial applications. Firstly, it is employed in film protection to shield molten metals, such as magnesium, from oxidizing when exposed to the surrounding air [10, 11]. Secondly, SF_6 plays a pivotal role in plasma etching, a critical step in the production of various technological components, including photovoltaic devices, integrated circuits, micro-electromechanical systems, and flat-panel displays [12]. Given its relatively high cost, SF_6 is often combined with other inert gases, such as nitrogen (N_2), and utilized in a diluted form across most applications. However, in semiconductor industries, where the demand for high-purity SF_6 remains significant, undiluted SF6 is still crucial [13]. This blending of SF_6 with other gases is a common practice to optimize cost-effectiveness while maintaining desired performance characteristics. It is worth noting that the use of mixed gases containing SF_6 is particularly prominent in regions with temperate climates. In these areas, there is a heightened risk of SF6 condensation at low ambient temperatures, typically ranging from below –30 °C to –40 °C. This condensation poses a challenge as it can lead to a decrease in

✉ Jabir H. Al-Fahemi
jhfahemi@uqu.edu.sa

✉ Kamal A. Soliman
kamalsoliman@gmail.com; kamal.soliman@fsc.bu.edu.eg

[1] Department of Chemistry, Faculty of Science, Umm Al-Qura University, 21955 Makkah, Saudi Arabia

[2] Department of Chemistry, Faculty of Science, Benha University, P.O. Box 13518, Benha, Egypt

the operational efficiency of SF_6 as a circuit breaker [14]. Some concerns about the harmful environmental effects of SF_6 have risen in recent years. SF_6 is a powerful greenhouse gas with a global warming potential (GWP) that is 23,500 times more than that of carbon dioxide (CO_2). This indicates that during 100 years, one molecule of SF_6 emitted into the atmosphere has the same warming impact as 23,500 molecules of CO_2 [15–18]. SF_6 is a highly long-lived gas, in addition to having a high GWP. SF_6 has an estimated atmospheric lifespan of 3,200 years [19]. This implies that SF_6 discharged into the atmosphere today will stay there for thousands of years, contributing to global warming. SF_6 is a substantial contributor to climate change due to its high GWP and long atmospheric lifespan. Global SF_6 emissions were expected to reach 8,300 metric tonnes in 2020. If no effort is made to reduce emissions, they are expected to rise to 14,000 metric tonnes by 2050. Small quantities of O_2 and H_2O react with SF_6 gas to produce low fluoride sulfide. Over time, internal insulation defects and aging within the gas-insulated switchgear (GIS) equipment can lead to partial discharges. These partial discharges can result in the breakdown of SF_6 gas, producing several stable gas species such as SO_2F_2, SOF_2, SO_2, and HF [20–25]. These decomposed gas species have a dangerous effect to human health and the environment negatively impact the insulating properties of SF_6 gas and can lead to the failure of GIS [26–32]. To ensure the stable operation of GIS and the entire power industry, it is crucial to identify GIS faults through continuous, real-time monitoring of SF_6 decomposition products within the GIS. This proactive monitoring helps maintain the reliability of the GIS system and the power sector as a whole.

In recent years, the world of two-dimensional (2D) materials, a field that has sparked extensive interest and innovation due to the unique chemical and physical properties, such as high specific surface area, excellent mechanical properties, relatively large carrier mobility, and good thermal conductivity [33–37]. Therefore, 2D nanomaterials have been utilized in many fields such as gas sensors [38–40], energy storage [41–44], electronic devices [45, 46], and catalysis [47, 48]. Computational studies based on density functional theory (DFT) were investigated to be potential in gas sensing for SF6 decomposition products, such as Co or Cr modified GeSe monolayer [8], $Ti_3C_2O_2$ MXene [49], InP3 monolayer [50], Pt-BN monolayer [51]. Pd modified C_3N_4 [52], and Sc-doped MoS_2 [53]. The research effort is primarily concerned with discovering low-cost 2D materials appropriate for usage in mobile devices, with attention to the environment synthesis processes. One material of interest is 2D SiGe with a honeycomb lattice, which has been theoretically explored and shown structural stability [54]. According to theoretical investigations, doped and functionalized 2D SiGe might be used as anodes in Li-ion batteries as well as hydrogen storage materials [55, 56]. Notably, recent publications show the effective synthesis of comparable nanostructures, emphasizing the necessity for additional investigation into the possibilities of this material. In this study, we used DFT calculations to examine the SiGe and Ca decorated SiGe monolayers for SF_6 decomposition gases. The novelty of this work lies in its innovative use of SiGe and Ca decorated SiGe for studying gas adsorption. This research has the potential to inform the development of advanced gas sensors and materials for a wide range of applications.

2 Computational details

All computations were performed in the framework of DFT as implemented in the DMol3 module of Materials Studio software code [57]. The study utilizes the Perdew-Burke-Engenho (PBE) function in the context of the generalized gradient approximation (GGA) to investigate electron exchange–correlation effects [58–60]. The Tkatchenko and Scheffler's (TS) method is employed to elucidate van der Waals forces, which play a crucial role in various molecular interactions [61]. A $4\times4\times1$ supercell of 2D SiGe, comprising 16 Si and 16 Ge atoms, to examine its ability to adsorb decomposed gases from sulfur hexafluoride (SF6). To minimize interference between neighboring structures, a vacuum region of 20 angstroms (Å) is incorporated into the supercell design. In the computational analysis, the double numerical plus polarization (DNP) method is employed with a basis set of 4.4, which accounts for the electron distributions and polarizabilities within the system [62]. The core-valence interaction was described by the semi-core pseudopotentials (DSPP) [63]. For geometric optimization and energy calculations, a Monkhorst–Pack k-point grid of $3\times3\times1$ was used, and $9\times9\times1$ for electronic structure calculations. The self-consistent field convergence accuracy (SCF tolerance) is set at 10^{-6} Ha (Hartrees), ensuring that the electronic structure calculations reach a level of precision necessary for reliable results. This parameter defines the threshold below which the SCF iterations are considered converged.

the binding energy $E_{binding}$ of Ca atom decorated the SiGe surface can be calculated by the following equation:

$$E_{binding} = E_{Ca\$2D-SiGe} - E_{Ca} - E_{SiGe} \quad (1)$$

where the $E_{Ca\$2D-SiGe}$, E_{Ca}, andE_{SiGe} are defined as the total energy of the Ca atom on SiGe, the single Ca atom, and the SiGe surface, respectively.

the amount of charge transfer (Q_T) between the gas and the surface was determined by Hirschfeld analysis. The adsorption energy E_{ads} of every gas molecule on SiGe and Ca\$2D – SiGe surfaces was calculated by the following equation:

$$E_{ads} = E_{Gas/surface} - E_{Gas} - E_{Surface} \quad (2)$$

where $E_{Gas/surface}$, E_{Gas}, and $E_{Surface}$ are the total energy of gas molecules adsorbed on the (SiGe and Ca\$2D − SiGe) surface, the energy of isolated gas, and the energy of the (SiGe and Ca\$2D − SiGe) surface, respectively.

3 Results and discussion

3.1 Structures of the target gas, 2D-SiGe, and Ca decorated SiGe

The geometry structures of the desired gas molecules (SF_6, SO_2F_2,SOF_2, SO_2, and HF) are presented, as seen in Fig. 1. The optimized SF6 molecule has an octahedral structure with a length of 1.611 Å between the S atom and the F atom. The S_2OF_2 and SOF_2 molecule has a tetrahedral structure, the bond lengths between S–O, and S-F are 1.431 Å, and 1.595 Å respectively. The bond angle between O-S-F is 107.969°. SOF_2 molecule has a pyramidal structure with Cs symmetry, the bond distances between S–O, and S-F are 1.446 Å, and 1.649 Å respectively. The bond angle between O-S-F is 106.794°. The SO_2 molecule exhibits a clear V-shaped structure. The distance between the O and S atoms is 1.464 Å, while the bond angle of O–S–O is 119.537°. The bond distance for H-F in the HF molecule is 0.934 Å. The structures of 2D-SiGe are depicted in Fig. 2, the computed lattice parameter is a = b = 3.94 Å along with a buckling value of 0.60 Å that is in agreement with the previous study [64]. Additionally, the Si–Ge covalent bond exhibits a length of 2.35 Å, and the bond angle for Ge-Si-Ge is measured at 113.694°. These findings offer important information regarding the material's geometric features and bonding configuration.

In order to determine the most stable geometry structure of a single Ca atom decorated pristine 2D-SiGe monolayer (Ca\$2D-SiGe). Figure 2, shows the optimal geometric structure of (Ca\$2D-SiGe). The Ca atom rests on a hollow site, which is positioned above the hexagonal hole, is the most

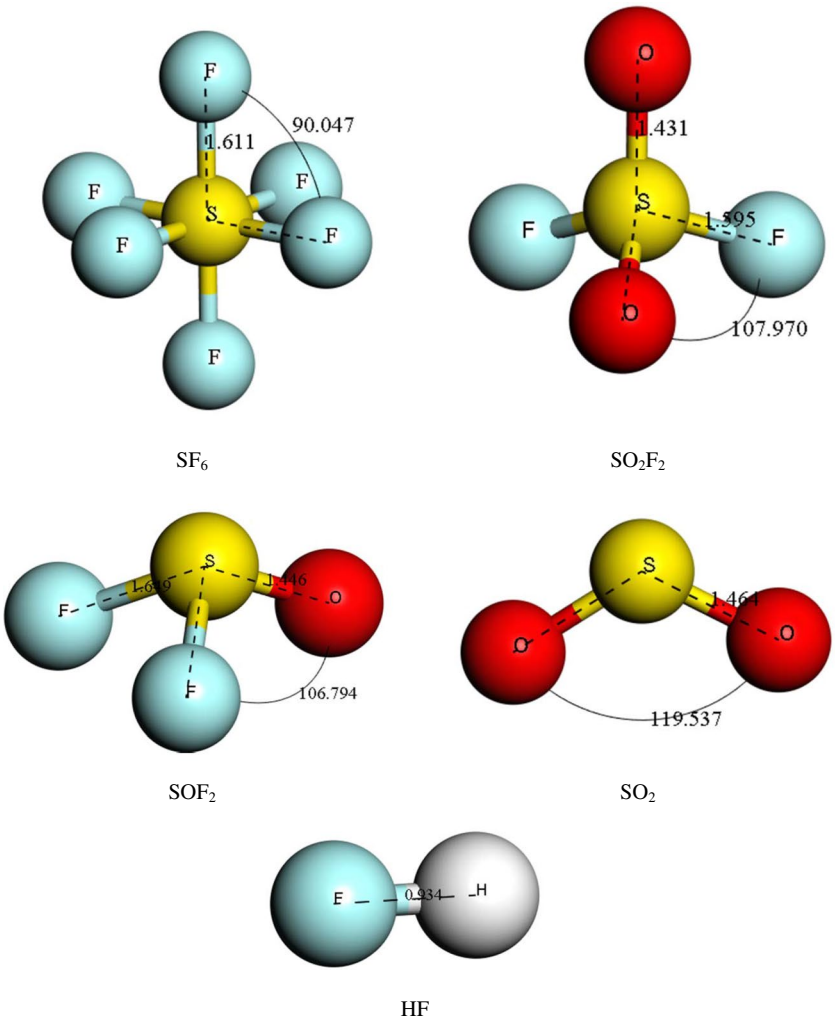

SF_6 SO_2F_2 SOF_2 SO_2 HF

Fig. 1 Optimized structures of the studies gases

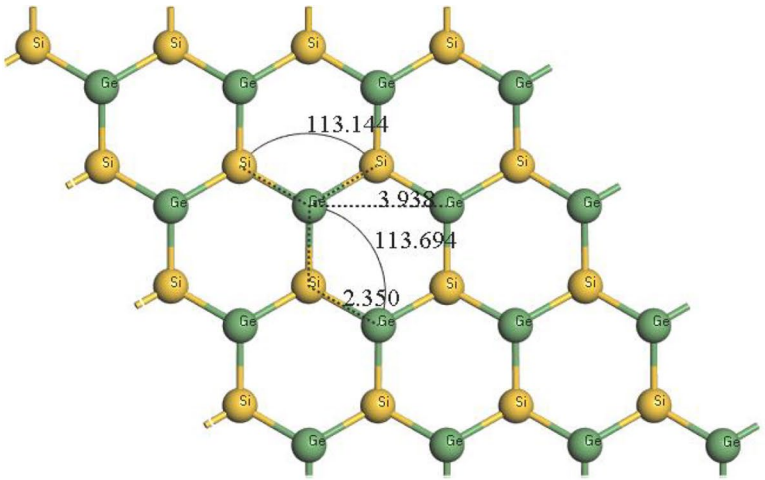

Top view of SiGe

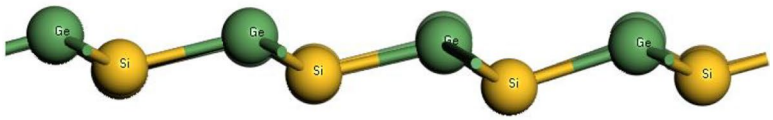

Side view of SiGe

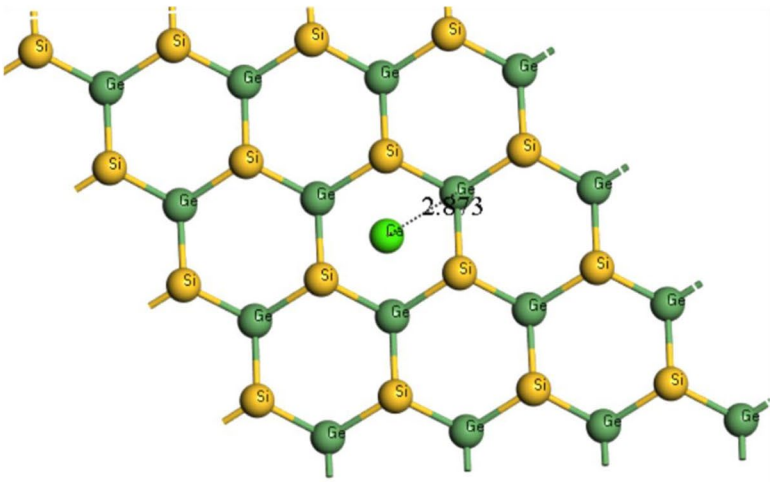

Top view of Ca$2D-SiGe

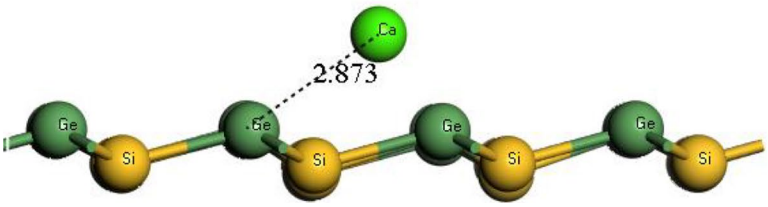

Side view of Ca$2D-SiGe

Fig. 2 The optimized structure of SiGe, and Ca decorated SiGe

Table 1 The parameters of SiGe and Ca decorated SiGe

	SiGe	Ca$2S-SiGe
Lattice constant (Å)	3.94	-
d (Å)	2.35 (Si-Ge)	2.873 (Ca-Ge)
E_b (eV)	-	-2.30
Q(e)	-	0.53

stable location, according to the binding energy results as seen in Table 1. The crystalline cohesive energy of 1.84 eV [65] is less than the binding energy of Ca, which is -2.30 eV. The distance between the Ca atom and the nearest neighbor Ge atom is 2.873 Å. The interaction of Ca with 2D-SiGe monolayer was investigated by Hirshfeld charge analysis. As presented in Table 1, the electronic charge on Ca atom has a positive sign that indicates the electron transferred from the Ca atom to the pristine 2D-SiGe.

3.2 Adsorption structures

This study extensively considers various adsorption forms of molecules. Figures 3 and 4, clearly represent the optimized and stable adsorption configurations. Key parameters such as adsorption energy, charge transfer, and the distance between SiGe, Ca$2D-SiGe, and adsorbed gases are systematically summarized in Table 2. SF6 molecule chemically adsorbs onto the two SiGe and Ca$2D-SiGe surfaces. As shown in Fig. 3, the SF6 molecule is still in octahedral form after adsorbing on the SiGe surface. The most stable SF6 adsorption over the SiGe surface exhibits the adsorption energy (E_{ads}) of -1.52 eV as presented in Table 2. The adsorption distance between the F atom of SF_6 and the Ge atom of the substrate is 3.424 Å. The amount of charge transfer obtained from Hirshfeld charge analysis is -0.0089 e, which demonstrates the charge transfer from the SiGe substate to the SF_6 molecule, revealing that the S atom of the SF_6 molecule loses an electron, while the six F atoms gain the electron. However, the SF_6 molecule adsorbed on Ca$2D-SiGe undergoes decomposition to $*SF_5$ and F* (* is the adsorbed species). The one F in SF_6 shows an elongation of the bond S-F from 1.62 Å to 4.97 Å and binds to the surface with an adsorption distance of 2.007 Å. The SF_6 adsorption over Ca$2D-SiGe shows the highest adsorption energy of -6.12 eV on the Ca site. The adsorption distance between the F atom of SF_5* and the Ca site is 2.166 Å. The adsorption energy of the SF6 molecule on Ca$2D-SiGe is 4.03 times higher than adsorption over the SiGe surface and the amount of charge in the case of Ca$2D-SiGe is higher than SiGe surface. As seen in Table 2, we can find that the charge transferred from the Ca site to the SF_6 molecule. Upon analyzing the adsorption energy outcomes for SF_6 gas molecules, it is evident that the SF_6 system exhibits the most negative E_{ads}. This strong chemical interaction occurs between the SiGe and Ca$2D-SiGe monolayers and the SF6 molecule.

Table 2 The adsorption parameter of studied gases on SiGe monolayer

Configuration	Adsorption distance (Å)	E_{ads}(eV)	Hirshfeld charge (e)		Q_T (e)
SF6/SiGe	3.424 (F-Ge)	–1.52	0.5834	S	–0.0089
			–0.0999	F	
			–0.0999	F	
			–0.0987	F	
			–0.0975	F	
			–0.0958	F	
			–0.1005	F	
SO2F2/SiGe	3.649 (F-Ge)	–1.39	0.5426	S	0.011
			–0.2031	O	
			–0.2032	O	
			–0.0632	F	
			–0.0621	F	
SOF2/SiGe	1.813 (F-Ge)	–2.00	0.3229	S	–0.2614
	2.19 (O-Ge)		–0.1968	O	
			–0.1413	F	
			–0.2462	F	
SO2/SiGe	2.944 (S-Ge)	–1.62	0.3337	S	–0.1472
			–0.2418	O	
			–0.2391	O	
HF/SiGe	2.529 (H-Ge)	–1.36	–0.2266	F	–0.1093
			0.1173	H	

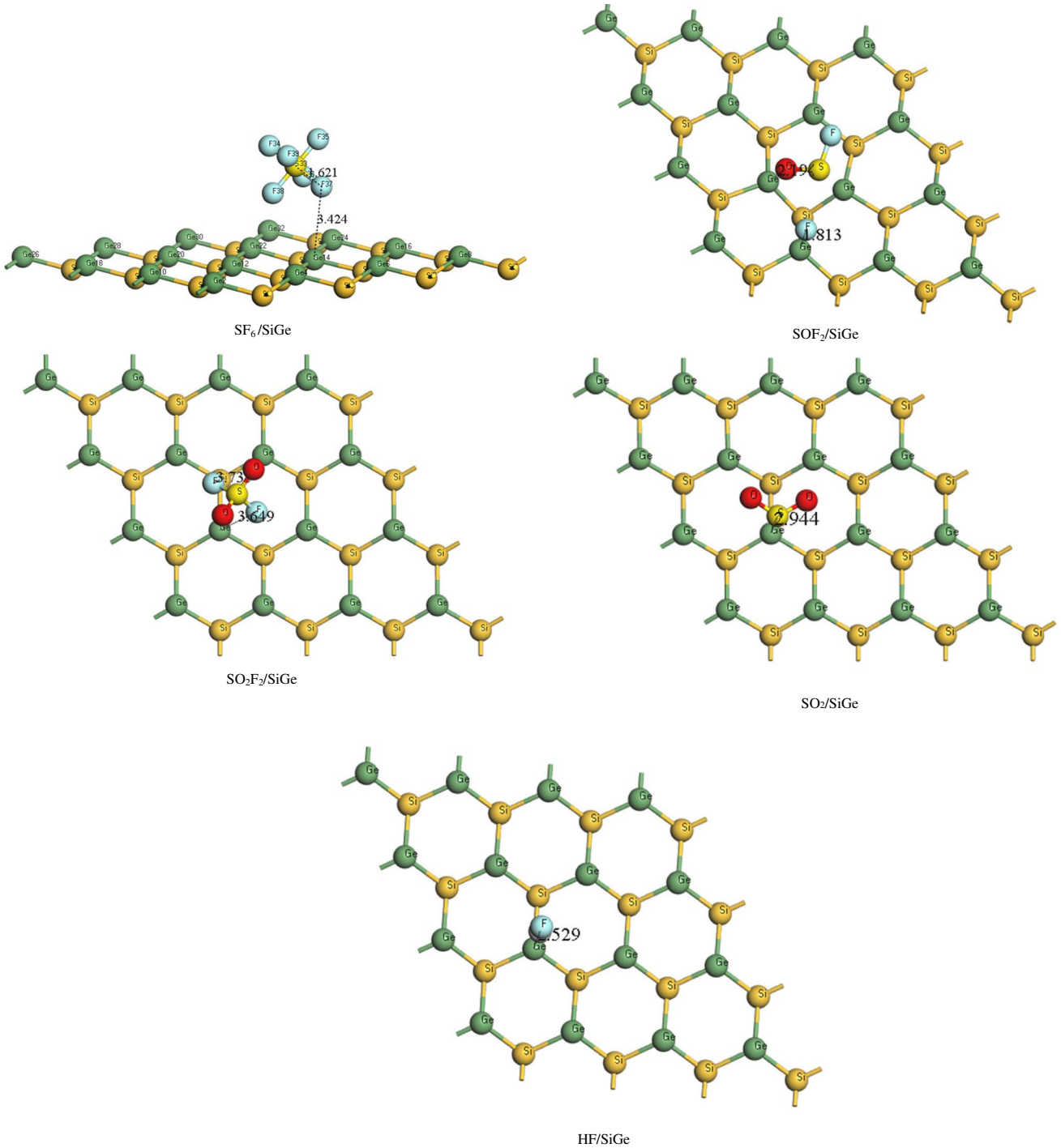

Fig. 3 Adsorption configurations of the studied gases on SiGe monolayer

The adsorption of SO_2F_2, and SOF_2 molecules on both SiGe and Ca$2D-SiGe surfaces that presented in Figs. 3 and 4, and the calculated parameters are collected in Tables 2 and 3. SO_2F_2 molecule interact with SiGe and Ca$2D-SiGe substrate via F atoms and the adsorption energies are -1.39 eV, and -5.66 eV for SiGe and Ca$2D-SiGe surfaces, respectively. In the case of a pristine SiGe monolayer, one F atom is located on hollow site and the other F atom is on top of the Si atom. The distance between Ge and F is 3.649 Å. While the SO_2F_2 adsorption on the Ca$2D-SiGe surface, the SO_2F_2 decomposes into SO_2* and 2F* leading to elongation of the two bonds of S-F to 5.164 Å and located on Ge atom of the substrate with distance 2.039 Å and the one O atom of SO_2F_2 interact with decorated Ca atom with distance 2.296 Å. By

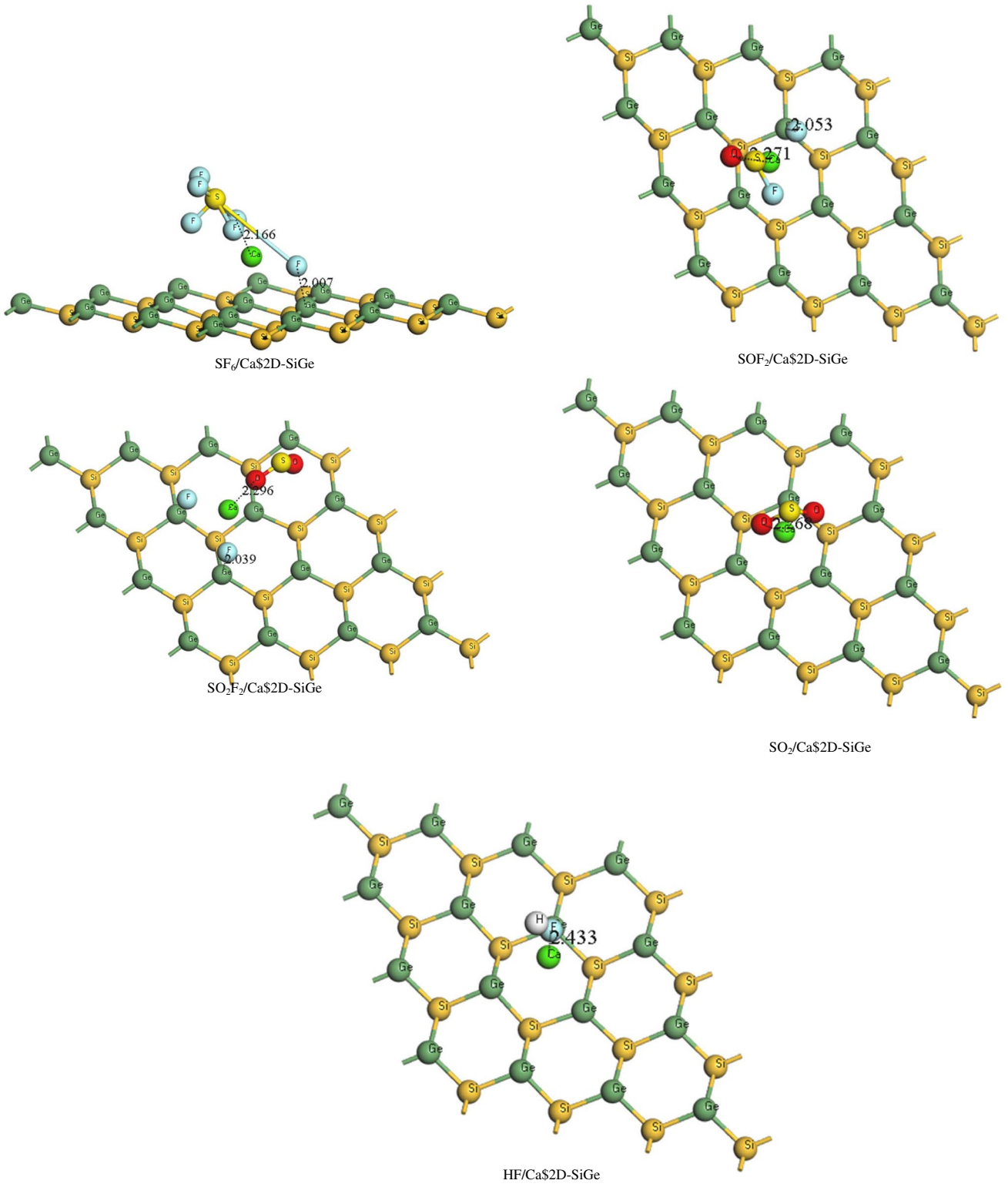

Fig. 4 Adsorption configurations of the studied gases on Ca$2D-SiGe monolayer

Hirshfeld charge analysis, it was found that 0.01 e transfers from SO_2F_2 molecule to SiGe substrate, while in Ca$2D-SiGe, the 0.635 e transfer from the Ca$2D-SiGe to SO_2F_2 leading to the strong interaction between Ca atom and O of SO_2F_2 molecule. Following the adsorption of SOF_2, Figs. 3 and 4 reveal the elongation of S-F bond in both SiGe and

Table 3 the adsorption parameter of studied gases on Ca$2D-SiGe monolayer

Configuration	Adsorption distance (Å)	E_{ads}(eV)	Hirshfeld charge (e)		Q_T(e)
SF6/Ca$2D-SiGe	2.007 (F-Ge)	-6.12	0.5601	S	-0.5495
	2.166 (F-Ca)		-0.0636	F	
			-0.1183	F	
			-0.2838	F	
			-0.2516	F	
			-0.2761	F	
			-0.1162	F	
SO2F2/ Ca$2D-SiGe	2.039 (F-Ge)	-5.66	0.3496	S	-0.635
	2.296 (O-Ca)		-0.2529	O	
			-0.2185	O	
			-0.2566	F	
			-0.2566	F	
SOF2/ Ca$2D-SiGe	2.296 (O-Ca)	-3.33	0.1834	S	-0.5412
			-0.2775	O	
			-0.2664	F	
			-0.1807	F	
SO2/ Ca$2D-SiGe	2.268 (O-Ca)	-2.22	0.26	S	-0.3305
			-0.2966	O	
			-0.2939	O	
HF/ Ca$2D-SiGe	2.433 (F-Ca)	-0.56	-0.0889	F	0.1815
			0.2704	H	

Ca$2D-SiGe surfaces. SOF_2 molecule was deformed after adsorption on the SiGe surface, and we found that from the shown in Fig. 3, this molecule was adsorbed parallel to the surface and the O-S-F angle changed from 106.79° to 104.82°. while SOF_2 molecule adsorbed on the Ca$2D-SiGe by the oxygen and fluorine atoms of SOF_2 molecule directed to the calcium decorated SiGe monolayer, where the other fluorine atom split and the distance between the sulfur and fluorine atoms became far away and approached the Ge atom of the substrate at a distance of 1.813 Å in case of SiGe and 2.053 Å for Ca$2D-SiGe surface. The adsorption energies of SOF2 molecules on both SiGe and Ca$2D-SiGe surfaces

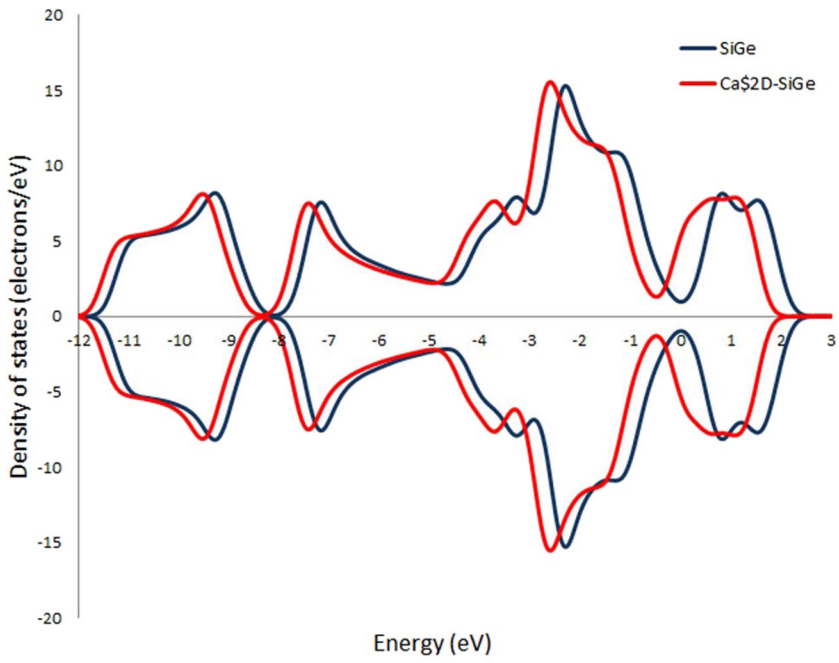

Fig. 5 DOS of SiGe and Ca$2D-SiGe surfaces

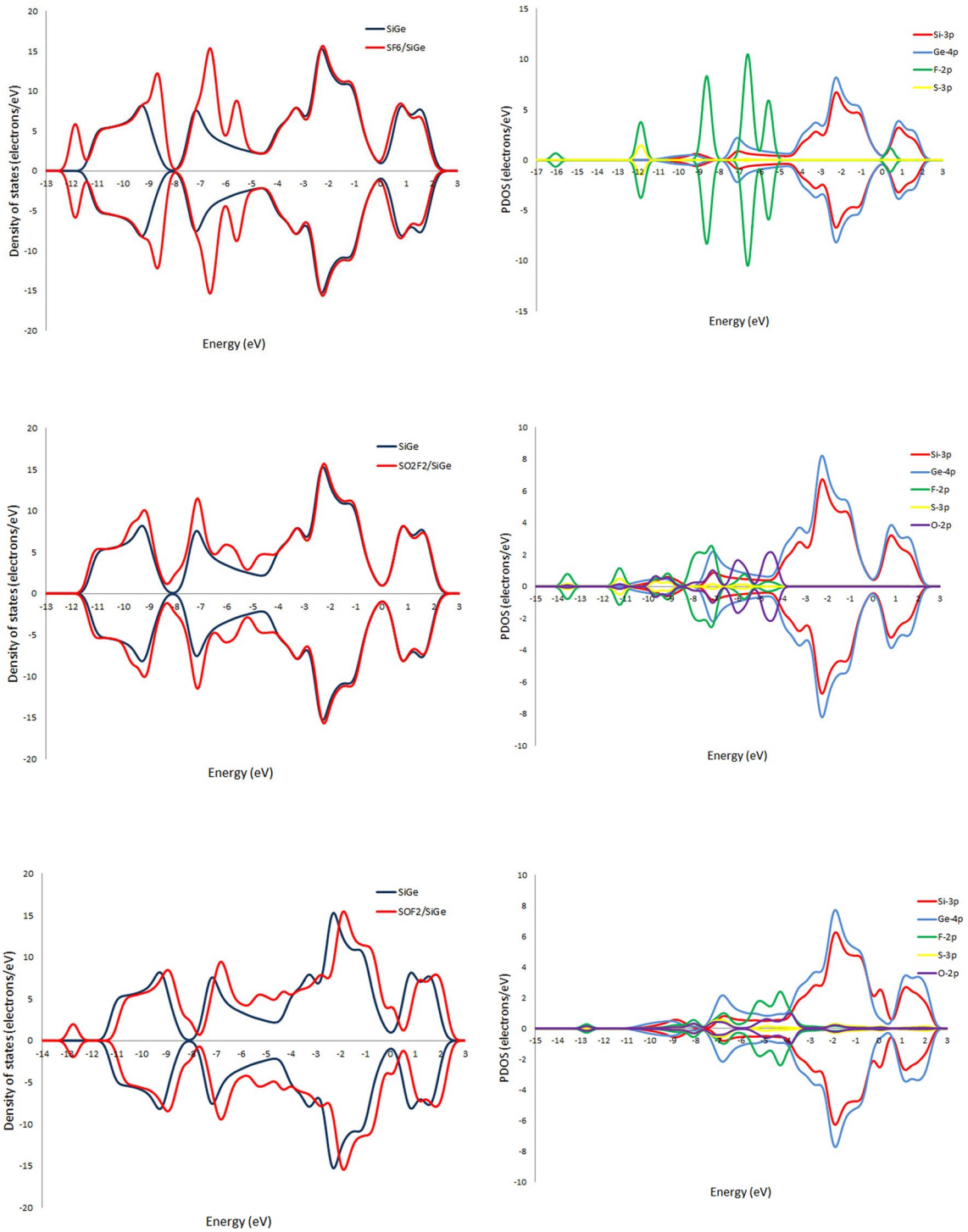

Fig. 6 DOS and PDOS of the studied gases on SiGe monolayer

are -2.00 eV and -3.33 eV, respectively. The charge transfer from SiGe and Ca decorated SiGe surfaces to the SOF2 molecule. The deformation of SOF_2 molecule is closely related to the amount of adsorption energy and charge transfer. After analyzing the forms of adsorption for both SO_2, and HF molecules on the SiGe and Ca$2D-SiGe surfaces, we found that the SO_2 molecule is adsorbed in parallel to SiGe as seen in Fig. 3, the adsorption energy as presented in Table 2, for this gas molecule is -1.62 eV and adsorption distance between S-Ge is 2.944 Å, while this molecule over Ca$2D-SiGe as shown in Fig. 4, the molecule has settled vertical and directed to the Ca decorated SiGe by the two oxygen atoms of SO_2.

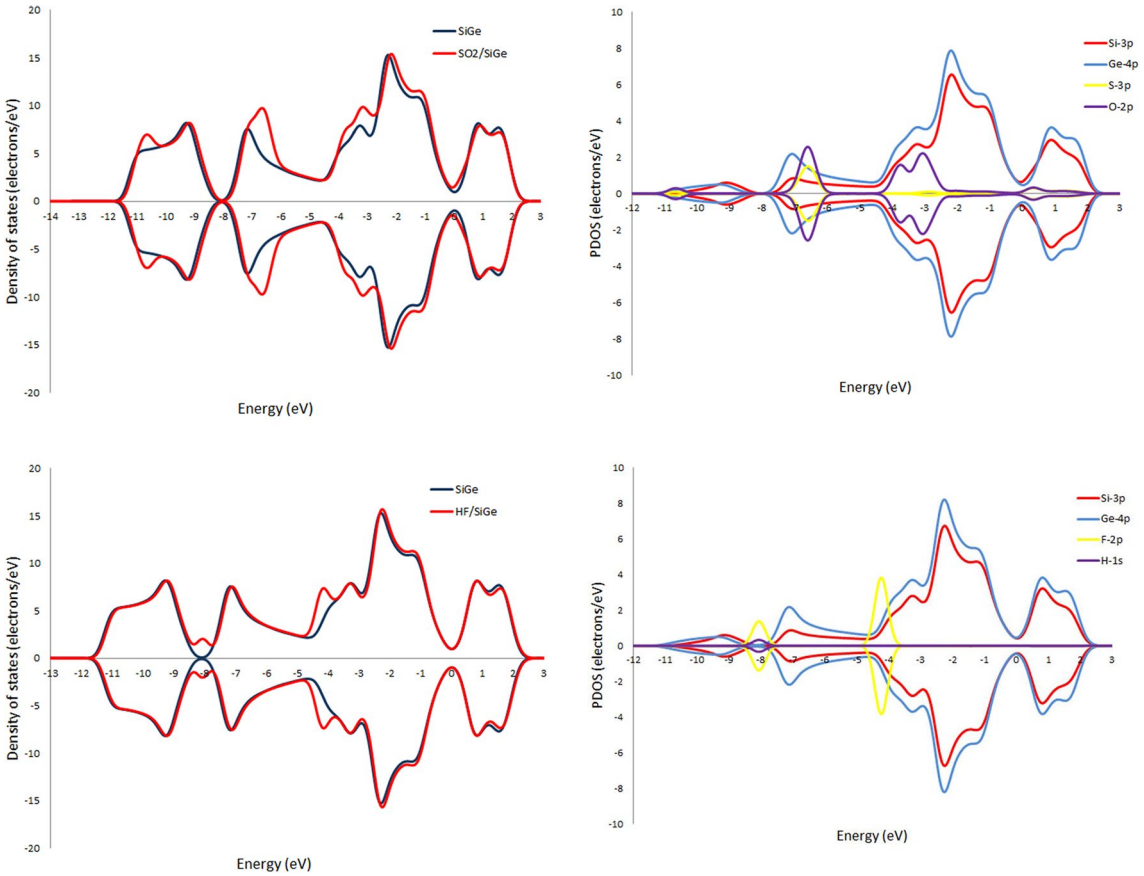

Fig. 6 (continued)

The adsorption energy for SO_2 on the Ca$2D-SiGe surface is -2.22 eV and the adsorption height between the O atom of SO_2 and the Ca atom is 2.268 Å. In the case of the interaction of HF molecules with SiGe and Ca$2D-SiGe surfaces, As presented in Fig. 2, the hydrogen atom of the HF molecule interacted with the SiGe surface with an adsorption energy of -1.36 eV, and adsorption distance H-Ge is 2.529 Å, but when this molecule interacted with the Ca$2D-SiGe surface, the molecule was rotated and the interaction took place between the F atom of HF molecule and Ca atom that is physically adsorbed with adsorption energy -0.56 eV, the distance between F atom and Ca atom is 2.433 Å and the angle of Ca-F–H is 137.73°. By analyzing the charge transfer as collected in Tables 2 and 3, the SO_2 molecule over SiGe and Ca$2D-SiGe surfaces act as electron acceptors as well as the HF molecule over SiGe surface, while the HF molecule on Ca$2D-SiGe surfaces acts as electron donors.

3.3 Electronic properties and electron density differences

The interaction of the Ca atom decorated SiGe monolayer reflects on the electronic properties through the density of states (DOS). The band gap for the decorated surface was decreased from 1.69 eV for SiGe to 1.23 eV for Ca$2D-SiGe and the peaks are shifted to the left, but the morphology of DOS doesn't change significantly as seen in Fig. 5. To uncover the microscopic sensing mechanism of the gases over SiGe, and Ca$2D-SiGe system, the DOS and projected density of states (PDOS) spectra of the SiGe, and Ca$2D-SiGe monolayers before and after gas adsorption are presented in Figs. 6 and 7. After the adsorption of SF_6 by the SiGe monolayer, as seen in Fig. 6 there are new peaks appeared near 0.17 eV, -5.70 eV, -6.68 eV, -8.70 eV, and -11.90 eV that is because of F-2p and Ge-4p orbitals, while for adsorption by Ca$2D-SiGe system as shown in Fig. 7, the DOS peaks are shifted to right and new peaks appear from -3.44 eV to -7.52 eV that there a strong overlap between Ca-3 s orbitals and F-2p orbitals at -3.56 eV, and -5.35 eV that resulting a strong adsorption of SF6 on the Ca$2D-SiGe surface. In the adsorption of SO_2F_2 and SOF_2 by SiGe surface, DOS changes a little for SO2F2 on SiGe surface, and for SOF_2 the peaks shifted to the right and the PDOS show the overlap at -7.46 eV between F-2p with Ge-4p orbitals for In SO_2F_2/SiGe and at -7.04 eV for SOF_2/SiGe, while a significant change of DOS for SO_2F_2

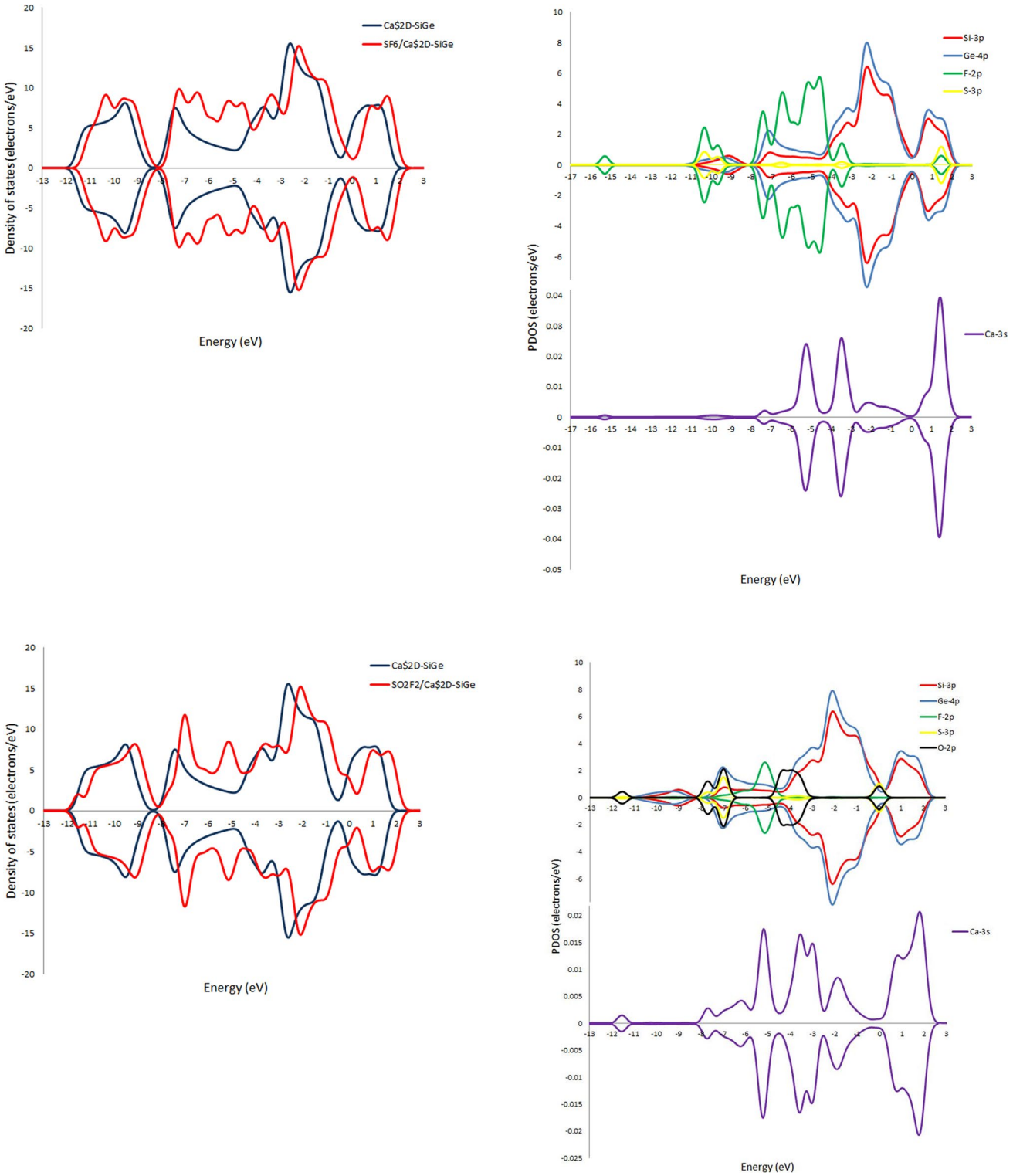

Fig. 7 DOS and PDOS of the studied gases on Ca$2D-SiGe monolayer

and SOF_2 on Ca$2D-SiGe surface. There is a big overlap between Ca-3 s and O-2p orbitals at -3.61 eV for SO_2F_2/ Ca$2D-SiGe and -5.13 eV, -6.38 eV for SOF_2/ Ca$2D-SiGe surfaces. As for the SO_2 and HF adsorption system, the peak values change slightly after the adsorption of SO_2, and HF gases. As seen in Fig. 6, there is the hybridization of O-2p,

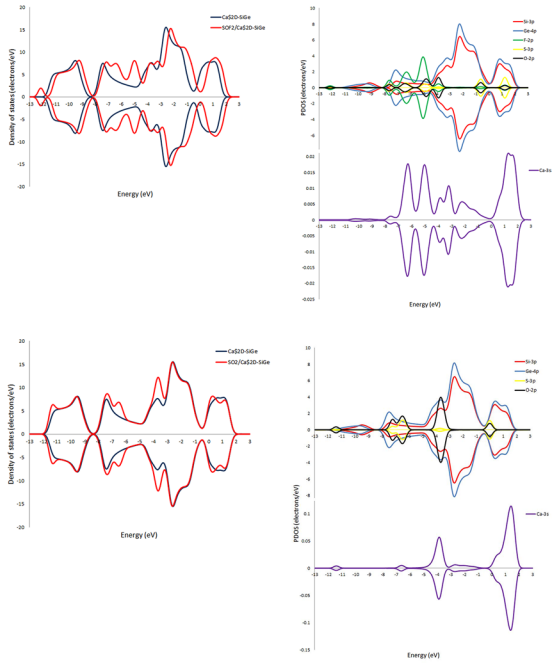

Fig. 7 (continued)

Si-3p, and Ge-4p at -3.92 eV for SO_2/SiGe, and the new peaks appear at -4.30 eV, and -8.18 eV for HF/SiGe surface. For DOS in Fig. 7, there is a little change after SO_2 and HF adsorbed on Ca$2D-SiGe. The PDOS shows the overlap O-2p and Ca-3 s orbitals at -3.96 eV and the new peaks appear at -9.05 eV and a little overlap signifying the weak adsorption between the HF molecule and Ca$2D-SiGe monolayer.

The electron density differences (EDD) analysis elucidates the nature of interactions between SF_6 decomposed gases and the monolayer system (SiGe, and Ca$2D-SiGe) as presented in Figs. 8 and 9. The blue and yellow colors represent electron depletion and accumulation, respectively. There is a charge depletion below the F atoms for SF_6, and HF systems, charge depletion below the O atoms for SO_2 systems, charge depletion below the O and F atoms for SO_2F_2 and SOF_2 systems, and charge accumulation between S-F atoms, S–O atoms, and Ca-SiGe substrate indicating electron transfer from S to F and O atoms and electron transfer from Ca decorated atom to substrate. In the case of HF/Ca$2D-SiGe, there is a limited charge transfer and charge accumulation between F and Ca atoms indicating charge transfer from HF to Ca$2D-SiGe monolayer.

3.4 Gas sensitivity and selectivity

The study explores the potential of SiGe and Ca$2D-SiGe as a gas sensor by examining adsorption properties such as adsorption energy and charge transfer. These properties influence changes in the density of states (DOS) and enhance electrical conductivity, crucial factors for a material to function efficiently as a gas sensor. Sensitivity, selectivity, and

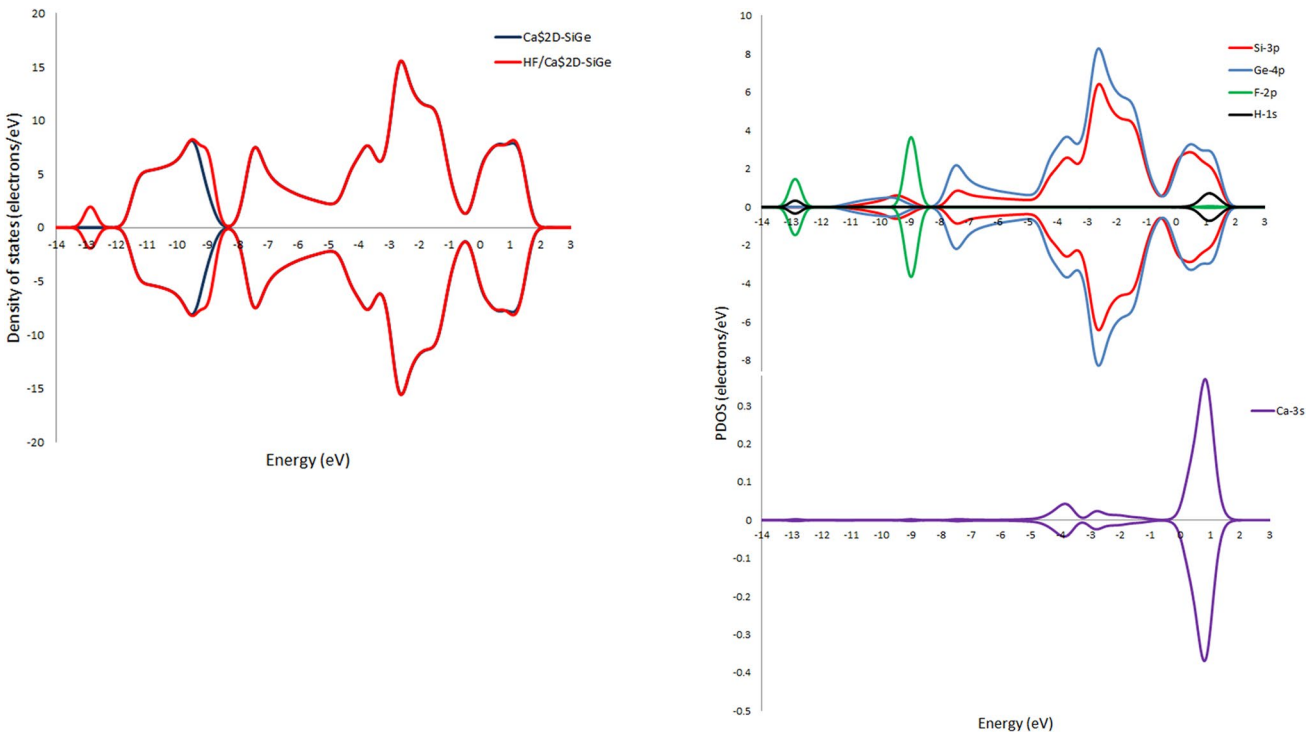

Fig. 7 (continued)

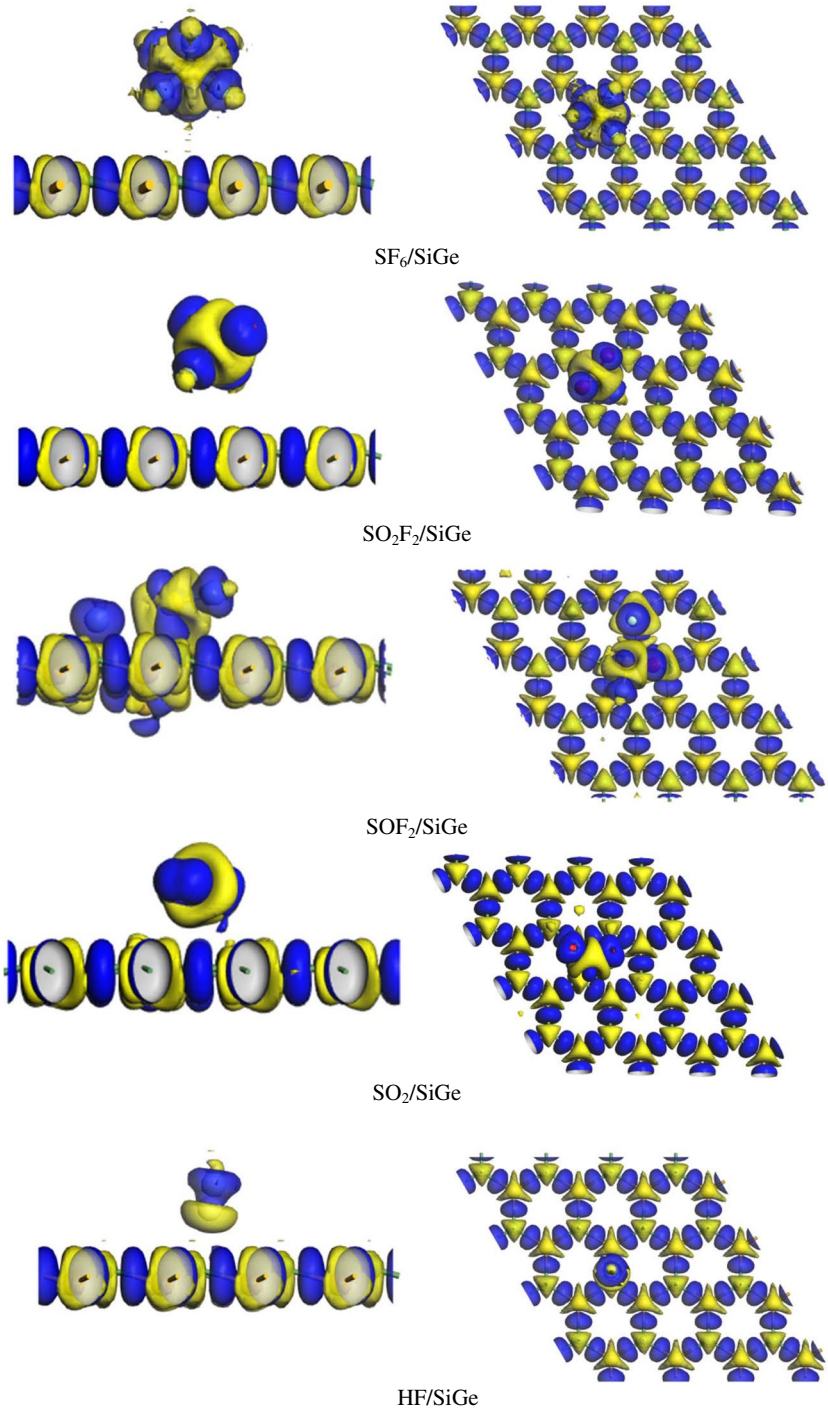

Fig. 8 EDD of the investigated gases on SiGe surface

recovery time are vital features in evaluating the effectiveness of a gas sensor [66, 67]. Sensitivity, a key parameter, is determined by observing the change in electrical conductivity (σ) before and after gas adsorption. The electrical conductivity of materials denoted as σ, and The sensitivity (S) of SiGe and Ca$2D-SiGe for gas adsorption can be calculated using following the provided formula [68, 69].

$$\sigma \propto exp^{(\frac{-E_g}{2K_BT})} \tag{3}$$

$$S = \left(\frac{1}{\sigma_{2D\_Gas}} - \frac{1}{\sigma_{2D}}\right)/(\frac{1}{\sigma_{2D}}) \tag{4}$$

where E_g, K_B, T are the band gap, Boltzmann's constant, and absolute temperature, respectively. $\sigma_{2D\_Gas}, \sigma_{2D}$ is the conductivity of the gas adsorbed system and isolated (SiGe and Ca$2D-SiGe) monolayer, respectively [70].

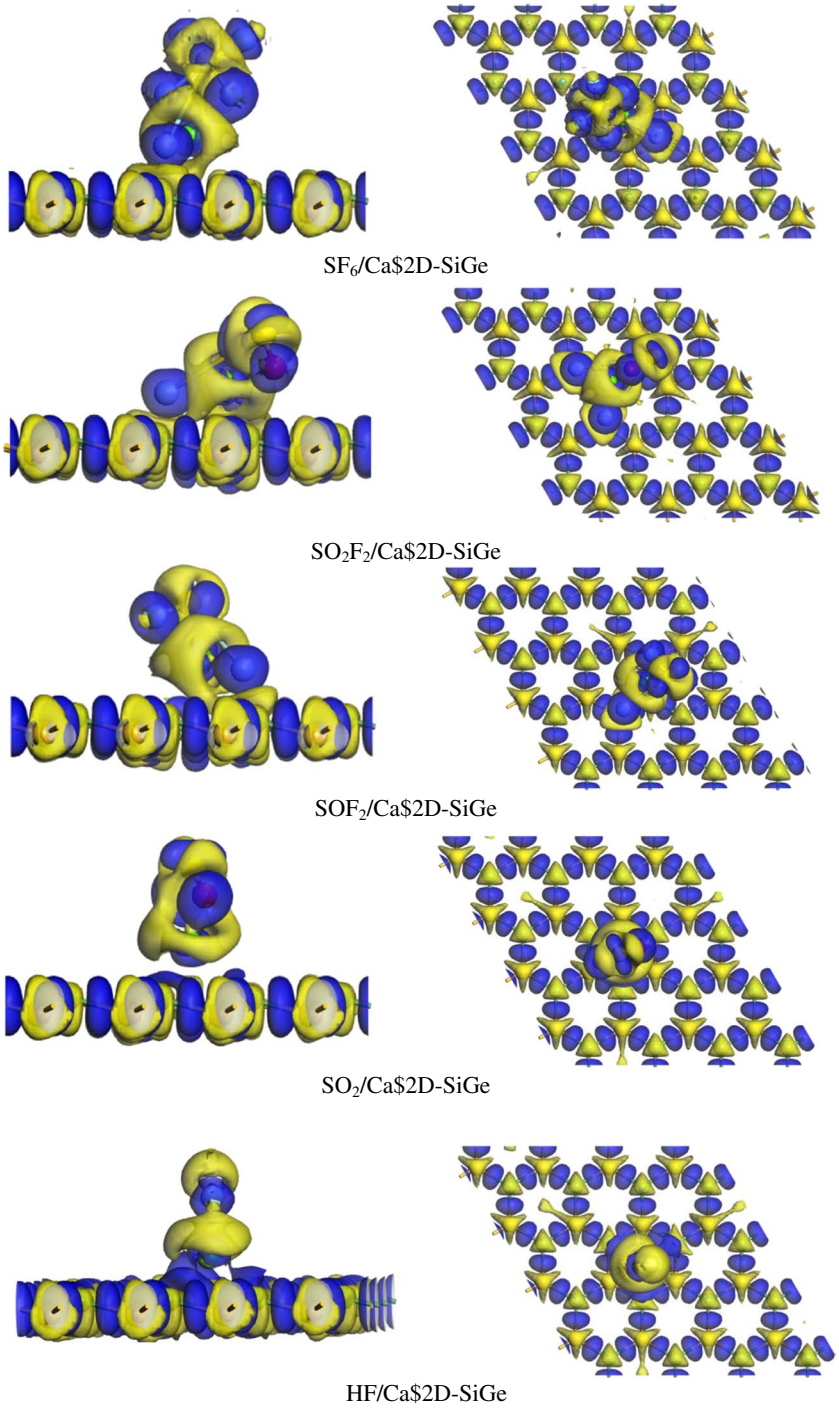

Fig. 9 EDD of the investigated gases on SiGe surface

The computed band gap of SiGe and Ca$2D-SiGe system are 1.69 eV, and 1.23 eV, respectively. After adsorbing gases, the band gap of SF_6, SO_2F_2, SOF_2, SO_2, and HF on SiGe is 1.31 eV, 1.61 eV, 0.12 eV, 1.22 eV, 1.59 eV, respectively. The band gap of SF_6, SO_2F_2, SOF_2, SO_2, and HF on Ca$2D-SiGe are 1.29 eV, 0.40 eV, 1.23 eV, 0.22 eV, and 0.13 eV, respectively. These gases except HF/ Ca$2D-SiGe showed chemical adsorption. Therefore, the SiGe and Ca$2D-SiGe substrate appeared as an efficient selectivity and sensing of gas molecules.

3.5 Recovery time

The time it takes for a gas to detach from the surface of the sensor material, known as recovery time, is a critical measure for evaluating sensing materials. This duration is influenced by the strength of the bond formed between the gas and the surface. Stronger bonds result in longer recovery times, making desorption challenging. Recovery time is calculated using the following formula [71]:

Table 4 The time recovery of studied gases on SiGe, and Ca$2D-SiGe surface at temperature 298 K, 698 K, and 898 K

Adsorption systems	$\tau atT = 298K$	$\tau atT = 698K$	$\tau atT = 898K$
SF_6/SiGe	4.99×10^{12}	9.36×10^{-3}	3.37×10^{-5}
SO_2F_2/SiGe	3.17×10^{10}	1.08×10^{-3}	6.29×10^{-6}
SOF_2/SiGe	6.05×10^{20}	27.30	1.66×10^{-2}
SO_2/SiGe	2.45×10^{14}	4.94×10^{-2}	1.23×10^{-4}
HF/SiGe	1.45×10^{10}	7.74×10^{-4}	4.86×10^{-6}
SF_6/ Ca$2D-SiGe	2.94×10^{90}	1.50×10^{31}	2.17×10^{21}
SO_2F_2/ Ca$2D-SiGe	3.34×10^{82}	6.06×10^{27}	5.00×10^{18}
SOF_2/ Ca$2D-SiGe	1.99×10^{43}	1.09×10^{11}	4.82×10^{5}
SO_2/ Ca$2D-SiGe	3.41×10^{24}	1.06×10^{3}	0.29
HF/ Ca$2D-SiGe	4.33×10^{-4}	1.30×10^{-9}	1.57×10^{-10}

$$\tau = A^{-1} exp^{\frac{-E_{ads}}{K_B T}} \quad (5)$$

where A is the attempt frequency ($10^{12} s^{-1}$), K_B is the Boltzmann's constant ($8.62 \times 10^{-5} eVK^{-1}$), and T is absolute the temperature [72]. The formula indicates that as the absolute value of adsorption energy decreases and the temperature increases, the duration for the gas to dissociate from the adsorbent surface becomes shorter. This observation is derived from the adsorption energy results. The time recovery of the SF_6 decomposition gases on the SiGe, and Ca$2D-SiGe surfaces are calculated at various temperatures (298 K, 698 K, and 898 K), and the results are shown in Table 4.

It can be seen that HF molecules on the Ca$2D-SiGe monolayer have the shortest time to desorb from the Ca$2D-SiGe surface. However, the other Four gases on the Ca$2D-SiGe surface have high adsorption energy, which results in an extended recovery time that does not meet the rapidity requirement for the sensing material. Hence, the Ca$2D-SiGe demonstrates significant potential as an adsorbent for these four gases (SF_6, SO_2F_2, SOF_2, and SO_2). At a temperature of 698 K, the HF on Ca$2D-SiGe, and all gases on the SiGe surface have a short time to detach from the monolayer surface. Moreover, with an increase in temperature (898 K), the duration for the desorption of HF from Ca$2D-SiGe and all gases on the SiGe surface are significantly reduced, indicating the potential for detecting these gas molecules.

4 Conclusion

The results reveal that SF_6 chemically adsorbs onto SiGe and Ca$2D-SiGe surfaces, with the latter exhibiting significantly higher adsorption energy and charge transfer. SO_2F_2 and SOF_2 molecules also show distinct adsorption behaviors, with the Ca$2D-SiGe surface demonstrating stronger interactions. HF adsorption on Ca$2D-SiGe results in a distinctive configuration, that demonstrates electron donor characteristics. Electronic property analysis through DOS and electron density differences provides valuable insights into the changes induced by gas adsorption. The study highlights the potential of Ca$2D-SiGe as an efficient gas sensor, demonstrating selectivity and sensitivity for all gas molecules. The recovery time analysis at different temperatures further underscores the suitability of Ca$2D-SiGe for gas detection applications. Overall, this investigation contributes to the understanding of the interactions between gas molecules and SiGe-based materials, offering promising prospects for gas sensing applications.

Author contributions **Jabir H. Al-Fahemi** and **Kamal A. Soliman** conceived of the idea. **Jabir H. Al-Fahemi and Kamal A. Soliman** analyzed data, wrote the manuscripts, and reviewed the present manuscript before its being submitted.

Funding This research received no external funding. All expenses associated with the design, execution, and publication of this study were borne by the authors. We declare that the absence of funding did not impact the integrity, objectivity, or impartiality of the research findings presented in this paper.

Data availability Not applicable.

Declarations

Competing interests The authors declare no competing interests.

Ethical approval We certify that we participated in the design of this work as well as the writing of the manuscript, and to assume public responsibility for it. We have reviewed the final version of the manuscript and we have agreed to publish this manuscript. This manuscript has not been published elsewhere. All authors are aware and agree to transmission, and no part of the manuscript has previously been published in another journal.

References

1. Scholz, A.-W., et al.: Comparison of magnetic resonance imaging of inhaled SF6 with respiratory gas analysis. Magn. Reson. Imaging **27**(4), 549–556 (2009)
2. Huang, H., Yu, Y., Zhang, M.: Analysis of adsorption properties of SF6 decomposed gases (SOF2, SO2F2, SF4, CF4, and HF) on Fe-doped SWCNT: A DFT study. Appl. Surf. Sci. **505**, 144622 (2020)
3. Shi, Z., et al.: A DFT study on adsorption of SF6 decomposition gases (H2S, SO2, SO2F2 and SOF2) on Sc-MoTe2 monolayer. Sens. Actuators, A **360**, 114548 (2023)
4. Li, S., et al.: Adsorption behaviors of SF6 decomposition gas on Ni-doped ZIF-8: A first-principles study. Vacuum **187**, 110131 (2021)
5. Yin, X., et al.: Compact QEPAS humidity sensor in SF6 buffer gas for high-voltage gas power systems. Photoacoustics **25**, 100319 (2022)
6. Yao, W., et al. A Classification System for Insulation Defect Identification of Gas-Insulated Switchgear (GIS), Based on Voiceprint

Recognition Technology. Applied Sciences, **10** (2020). https://doi.org/10.3390/app10113995
7. Han, X., et al.: Study on the combined characteristics of UHF and optical signals induced by partial discharge at spacer surface in GIS. IET Gener. Transm. Distrib. **14**(16), 3332–3337 (2020)
8. Chen, J., et al.: Adsorption and gas-sensing properties of SF6 decomposition components (SO2, SOF2 and SO2F2) on Co or Cr modified GeSe monolayer: a DFT study. Mater. Today Chem. **28**, 101382 (2023)
9. Kong, L., et al.: Adsorption of SF6 Decomposed Species on Ti3C2O2 and Ti3C2F2 with Point Defects by DFT Study. Adv. Theor. Simul. **4**(7), 2100074 (2021)
10. Chuah, C.Y., et al.: Enhanced SF6 recovery by hierarchically structured MFI zeolite. J. Ind. Eng. Chem. **62**, 64–71 (2018)
11. Chuah, C.Y., Lee, Y., Bae, T.-H.: Potential of adsorbents and membranes for SF6 capture and recovery: A review. Chem. Eng. J. **404**, 126577 (2021)
12. Fang, X., et al.: Sulfur Hexafluoride (SF6) Emission Estimates for China: An Inventory for 1990–2010 and a Projection to 2020. Environ. Sci. Technol. **47**(8), 3848–3855 (2013)
13. Kim, K., et al.: Status of SF6 separation/refining technology development for electric industry in Korea. Sep. Purif. Technol. **200**, 29–35 (2018)
14. Kui, L.W., et al.: Analysis and experimental study on liquefaction characteristics of SF6/CF4 mixture gas. In: 2017 4th International Conference on Electric Power Equipment - Switching Technology (ICEPE-ST), pp. 305–309. (2017)
15. Dervos, C.T., Vassiliou, P.: Sulfur hexafluoride (SF6): global environmental effects and toxic byproduct formation. J. Air Waste Manag. Assoc. **50**(1), 137–141 (2000)
16. Tsai, W.-T.: The decomposition products of sulfur hexafluoride (SF6): Reviews of environmental and health risk analysis. J. Fluorine Chem. **128**(11), 1345–1352 (2007)
17. Parthiban, A., et al.: Disposal methods, health effects and emission regulations for sulfur hexafluoride and its by-products. J. Hazard. Mater. **417**, 126107 (2021)
18. Reilly, J., et al.: Multi-gas assessment of the Kyoto Protocol. Nature **401**(6753), 549–555 (1999)
19. Forster, P., et al.: Chapter 7: The Earth's energy budget, climate feedbacks, and climate sensitivity. In: Open Access Te Herenga Waka-Victoria University of Wellington. (2021)
20. Rabie, M., Franck, C.M.: Assessment of Eco-friendly Gases for Electrical Insulation to Replace the Most Potent Industrial Greenhouse Gas SF6. Environ. Sci. Technol. **52**(2), 369–380 (2018)
21. Marzouk, S.A.M., Al-Marzouqi, M.H.: Analyzer for continuous monitoring of H2S in gas streams based on a novel thermometric detection. Sens. Actuators, B Chem. **162**(1), 377–383 (2012)
22. Gao, X., et al.: Adsorption of SO2 molecule on Ni-doped and Pd-doped graphene based on first-principle study. Appl. Surf. Sci. **517**, 146180 (2020)
23. Zeng, F., et al.: Study on the influence mechanism of trace H2O on SF6 thermal decomposition characteristic components. IEEE Trans. Dielectr. Electr. Insul. **22**(2), 766–774 (2015)
24. Xiao, S., et al.: The influence of Cu, Al and Fe free metal particles on the insulating performance of SF6 in C-GIS. IEEE Trans. Dielectr. Electr. Insul. **24**(4), 2299–2305 (2017)
25. Wang, J., et al.: Highly sensitive multi-pass cavity enhanced Raman spectroscopy with novel polarization filtering for quantitative measurement of SF6 decomposed components in gas-insulated power equipment. Sens. Actuators, B Chem. **380**, 133350 (2023)
26. Zhang, X., Meng, F., Yang, B.: Use of hydroxyl-modified carbon nanotubes for detecting SF6 decomposition products under partial discharge in gas insulated switchgear. IEEE Trans. Dielectr. Electr. Insul. **20**(6), 2246–2253 (2013)
27. Liu, H., et al. Synthesis, Characterization and Enhanced Sensing Properties of a NiO/ZnO p–n Junctions Sensor for the SF6 Decomposition Byproducts SO2, SO2F2, and SOF2. Sensors, 2017. **17**. https://doi.org/10.3390/s17040913
28. Sulbaek Andersen, M.P., et al.: Atmospheric Chemistry of (CF3)2CF–C≡N: A Replacement Compound for the Most Potent Industrial Greenhouse Gas, SF6. Environ. Sci. Technol. **51**(3), 1321–1329 (2017)
29. Chu, J., et al.: Highly selective detection of sulfur hexafluoride decomposition components H2S and SOF2 employing sensors based on tin oxide modified reduced graphene oxide. Carbon **135**, 95–103 (2018)
30. Taha, R.A., et al.: DFT study of adsorbing SO2, NO2, and NH3 gases based on pristine and carbon-doped Al24N24 nanocages. J. Mol. Model. **29**(5), 140 (2023)
31. Soliman, K.A., Aal, S.A.: The efficiency of n- and p-type doping silicon carbide nanocage toward (NO2, SO2, and NH3) gases. Chem. Pap. **76**(8), 4835–4853 (2022)
32. Fadlallah, M.M., Maarouf, A.A., Soliman, K.A.: Boron nitride nanocones template for adsorbing NO2 and SO2: An ab initio investigation. Physica E **113**, 188–193 (2019)
33. Mir, S.H., Yadav, V.K., Singh, J.K.: Recent Advances in the Carrier Mobility of Two-Dimensional Materials: A Theoretical Perspective. ACS Omega **5**(24), 14203–14211 (2020)
34. Baig, N.: Two-dimensional nanomaterials: A critical review of recent progress, properties, applications, and future directions. Compos. A Appl. Sci. Manuf. **165**, 107362 (2023)
35 Kumbhakar, P., et al.: Prospective applications of two-dimensional materials beyond laboratory frontiers: A review. iScience **26**(5), 106671 (2023)
36. Khandelwal, G., et al.: Recent developments in 2D materials for energy harvesting applications. Journal of Physics: Energy **5**(3), 032001 (2023)
37. Park, S., Ruoff, R.S.: Chemical methods for the production of graphenes. Nat. Nanotechnol. **4**(4), 217–224 (2009)
38. Donarelli, M. and L. Ottaviano 2D Materials for Gas Sensing Applications: A Review on Graphene Oxide, MoS2, WS2 and Phosphorene. Sensors. **18** (2018). https://doi.org/10.3390/s18113638.
39. Rajkumar, K., Kumar, R.T.R.: Chapter 6 - Gas Sensors Based on Two-Dimensional Materials and Its Mechanisms. In: Hywel, M., Rout, C.S., Late, D.J. (eds.) Fundamentals and Sensing Applications of 2D Materials, pp. 205–258. Woodhead Publishing (2019)
40. Maryam, B., Bharati, T.: Two-dimensional materials for gas sensors: from first discovery to future possibilities. Surface Innovations **6**(4–5), 205–230 (2018)
41. Khan, K., et al.: Recent advances in two-dimensional materials and their nanocomposites in sustainable energy conversion applications. Nanoscale **11**(45), 21622–21678 (2019)
42. Lee, S., Jung, S.C., Han, Y.-K.: Fe2CS2 MXene: a promising electrode for Al-ion batteries. Nanoscale **12**(9), 5324–5331 (2020)
43. Petr, M., et al.: Thermally reduced fluorographenes as efficient electrode materials for supercapacitors. Nanoscale **11**(44), 21364–21375 (2019)
44. Xu, B., et al.: 2020 roadmap on two-dimensional materials for energy storage and conversion. Chin. Chem. Lett. **30**(12), 2053–2064 (2019)
45. Kaushal, P., Khanna, G.: The role of 2-Dimensional materials for electronic devices. Mater. Sci. Semicond. Process. **143**, 106546 (2022)
46. Chi, S., et al.: A DFT study of the adsorption of noble metal adatoms (Pd, Pt, Ag, Au) on 2D tin disulfide monolayers: Potential towards nanoscale electronic devices. Physica E **120**, 114080 (2020)
47. Liu, D., et al.: Single noble metal atoms doped 2D materials for catalysis. Appl. Catal. B **297**, 120389 (2021)

48 Zhu, H., et al.: DFT practice in MXene-based materials for electrocatalysis and energy storage: From basics to applications. Ceramics Int. **48**(19, Part A), 27217–27239 (2022)
49. Dong, A., Liu, M.: A DFT study on the adsorption properties of Ti3C2O2 MXene towards SF6 decomposition gases. Surf. Sci. **734**, 122317 (2023)
50. Liao, Y., et al.: Adsorption properties of InP3 monolayer toward SF6 decomposed gases: A DFT study. Physica E **130**, 114689 (2021)
51. Li, J.-Y., Wang, P., Akram, S.: Adsorption and sensing for SF6 decomposed gases by Pt-BN monolayer: a DFT study. Mol. Phys. **119**(14), e1950856 (2021)
52. Sun, M., Dong, A., Gui, Y.: Gas-sensing properties of Pb, Pd modified C3N4 for SF6 decomposition products detection: A DFT study. Chem. Phys. **570**, 111898 (2023)
53. Li, B., et al.: Adsorption of SF6 decomposition gases (H2S, SO2, SOF2 and SO2F2) on Sc-doped MoS2 surface: A DFT study. Appl. Surf. Sci. **549**, 149271 (2021)
54. Şahin, H., et al.: Monolayer honeycomb structures of group-IV elements and III-V binary compounds: First-principles calculations. Phys. Rev. B **80**(15), 155453 (2009)
55. Sannyal, A., Ahn, Y., Jang, J.: First-principles study on the two-dimensional siligene (2D SiGe) as an anode material of an alkali metal ion battery. Comput. Mater. Sci. **165**, 121–128 (2019)
56. Cid, B.J., et al.: Hydrogen storage on metal decorated pristine siligene and metal decorated boron-doped siligene. Mater. Lett. **293**, 129743 (2021)
57. Delley, B.: From molecules to solids with the DMol3 approach. J. Chem. Phys. **113**(18), 7756–7764 (2000)
58. Wang, X., Wang, J.: Effects of Pt and Au adsorption on the gas sensing performance of SnS2 monolayers: A DFT study. Mater. Sci. Semicond. Process. **121**, 105416 (2021)
59. Perdew, J.P., Wang, Y.: Accurate and simple analytic representation of the electron-gas correlation energy. Phys. Rev. B **45**(23), 13244–13249 (1992)
60. Liu, D., et al.: Adsorption of SF6 decomposition components over Pd (1 1 1): A density functional theory study. Appl. Surf. Sci. **465**, 172–179 (2019)
61. Cui, H., et al.: Ru-InN Monolayer as a Gas Scavenger to Guard the Operation Status of SF6 Insulation Devices: A First-Principles Theory. IEEE Sens. J. **19**(13), 5249–5255 (2019)
62. Cui, H., et al.: First-principles insight into Ni-doped InN monolayer as a noxious gases scavenger. Appl. Surf. Sci. **494**, 859–866 (2019)
63. Delley, B.: Hardness conserving semilocal pseudopotentials. Phys. Rev. B **66**(15), 155125 (2002)
64. Nguyen, D.K., et al.: Chemical functionalization of low-buckled SiGe monolayer: Effects on the electronic and magnetic properties. Mater. Sci. Semicond. Process. **150**, 106949 (2022)
65. Ataca, C., Aktürk, E., Ciraci, S.: Hydrogen storage of calcium atoms adsorbed on graphene: First-principles plane wave calculations. Phys. Rev. B **79**(4), 041406 (2009)
66. Zhang, J., et al.: Nanostructured Materials for Room-Temperature Gas Sensors. Adv. Mater. **28**(5), 795–831 (2016)
67. Isa, M., et al.: A DFT study of silver decorated bismuthene for gas sensing properties and effect of humidity. Mater. Sci. Semicond. Process. **145**, 106635 (2022)
68. Zhou, Q., et al.: Adsorption of H2S on graphane decorated with Fe, Co and Cu: a DFT study. RSC Adv. **7**(50), 31457–31465 (2017)
69. Moradi, M., Noei, M., Peyghan, A.A.: A theoretical study on surface modification of a nanosized BC3 tube using C2H4 and its derivatives. Struct. Chem. **25**(1), 221–229 (2014)
70. Li, S.S.: Semiconductor statistics. In: Semiconductor Physical Electronics, pp. 45–60. Springer (2006)
71. Noei, M.: Probing the electronic sensitivity of BN and carbon nanotubes to carbonyl sulfide: A theoretical study. J. Mol. Liq. **224**, 757–762 (2016)
72. Yamaguchi, K., et al.: A spin correction procedure for unrestricted Hartree-Fock and Møller-Plesset wavefunctions for singlet diradicals and polyradicals. Chem. Phys. Lett. **149**(5), 537–542 (1988)